19th Brazilian Congress of Thermal Sciences and Engineering
November 06th-10th, 2022, Bento Gonçalves - RS - Brazil

ENCIT-2022-0126
THERMAL DIFFUSIVITY AND SURFACE MECHANICAL PROPERTIES OF THE PLASMA NITRIDED HASTELLOY X SUPERALLOY

Regiane Gordia Drabeski
Rafael Fillus Chuproski
Isabel Borges da Rocha
State University of Ponta Grossa – Ponta Grossa, PR 84030-900, Brazil.
e-mails: regiane.drabeski@escola.pr.gov.br; rafaelchuproki@gmail.com; isabebel0321@gmail.com.

Daniele Toniolo Dias
Anderson Geraldo Marenda Pukasiewicz
Federal University of Technology - Parana, Ponta Grossa, PR 84016-210, Brazil.
e-mail: danieletdias@utfpr.edu.br

Gelson Biscaia de Souza
State University of Ponta Grossa – Ponta Grossa, PR 84030-900, Brazil.
e-mail: gelsonbs@uepg.br.

Abstract. *The nickel-based superalloy Hastelloy X were DC plasma nitrided for the first time in this study. Structure and mechanical properties of the nitrided surfaces were compared with the respective bulks, subjected only to heating. The nitriding produced the expanded austenite phase (mainly at 400 °C) and metal nitrides, such as Cr_2N (in the higher temperatures, 500-700 °C). The nitrogen diffusion in the matrix obeyed a complex and dynamic correlation with temperature due to the competitive nitrogen retention in interstices and precipitates. The thickest layer (8 μm) and nitrogen amount (20 at%) were attained at the 600 °C nitriding. The overall thermal effect in the superalloy bulk was the precipitation of S-phase at 700 °C, for which hardness increased from 3.8 to 4.3 GPa. The nitrogen inlet yielded strengthened cases, with hardness values reaching 10.5 GPa (at 400 °C) and ~14 GPa (at the remaining conditions). The thermal diffusivity of the superalloy was 1.86×10^{-6} m²/s. After the nitriding process, the effective thermal diffusivity values increased with the treatment temperature, reaching 4.31×10^{-6} m²/s at 700°C the maximum nitriding temperature, a value similar to that of commercially available Chromel. These results are of intrinsic importance for the load bearing capacity and heating dissipation of the modified surfaces.*

Keywords: *Photoacoustic Measurement, Phase-lag, Nanoindentation, Elastic Modulus.*

1. INTRODUCTION

Aircrafts are a means of transportation, work, and defense of great importance. From the structure, it is expected good durability and resistance to the working conditions. The materials science and engineering are the areas responsible for developing and improving the materials used in their construction and maintenance (Eriksson, 2013).

In flight conditions, the turbine works under high pressures and temperatures (>1000 °C). In addition, the turbine blades come into contact with dirt from the atmosphere the burning fuel. Both factors prompt the beginning of the corrosion process on the device. In order to attend the necessary working conditions, nickel superalloys are applied in the production of several parts of the aircraft turbines, as they have high temperature and corrosion resistances (Wang, 2011).

Superalloys are among the materials that have shown the greatest evolution in recent decades. Among the range of superalloys available, the ones made of nickel (Ni), Cobalt (Co) and Chromium (Cr) stand out, which are used, beside blades, in other engine components such as discs, combustion chamber, afterburners and thrust reversers (Zang, 2013; Mouritz, 2012).

The Hastelloy X nickel superalloy (Ni, 22%Cr, 18%Fe, 9%Mo, 1.5%Co, 0.6%W, by %wt), developed by Haynes International, has been used in the aerospace field for several decades. It is the subject of the present study.

The Hastelloy X superalloy is intended for both the combustion and exhaust stages, in components such as blades, ducts, combustors, fuel injectors and flame supports. In addition to aerospace applications, the Hastelloy superalloy also finds application in industrial gas turbines. The intrinsic properties of the alloy are not enough for such applications. Depositions of protective layers are necessary in order to avoid failures in components, such as in blades that occur due to the working conditions, with special focus on the thermal barrier coatings (TBC) (Kovářík et al., 2016). These, however, still lack of proper adhesion strength (Takahashi, Assis, Piorino, Reis, 2019).

To optimize the lifespan of aircraft turbines, it is compelling to develop intermediate layers between the bulk and the TBC, or simply find layers that replace it. Plasma nitriding is a thermochemical process with potential to promote mechanical and thermal stability to the surface through diffusion and retention of nitrogen in the material´s crystal structure (Alves, 2006; Dong, 2010). Thicknesses of the modified layers can vary from a few micrometers to tenths of a millimeter (Ceccareli, 2008; Manova et al., 2017). A residual stress gradient exist through the modified layer, resulting in an improved load bearing capacity under conditions of thermal or mechanical stresses to films deposited on them (Limiar, 2014, Sfar, et al., 2002).

Several authors have studied over the decades the nitriding of nickel superalloys, especially Inconel, by gaseous or plasma-assisted methods; some examples are Leroy et al. (2001), He et al. (2004), Dong (2010) and Kovaci et al. (2016). As far as it was possible to verify in the Brazilian scientific databases website (www.periodicos.capes.gov.br), there are still no studies regarding the Hastelloy nitriding.

The main product of the plasma nitriding carried out at low temperatures (<500 °C) in the Fe-Cr and Co-Cr superalloy series, as well as in austenitic steels (Ueda et al., 2014; Ueda et al., 2016), is the nitrogen supersaturated expanded austenite (or the S-phase), which result in surface layers with better mechanical, tribological and corrosion behaviors. The nitriding performed under higher temperatures originate metal-nitrogen compounds layers, which role in the surface protection is complex.

Equally important for protective layers on turbine devices are the thermal properties. In this regard, the thermal diffusivity of the Hastelloy X, with or without nitriding, are still to be studied. Actually, only one study in the literature hitherto investigated thermal diffusivity in a nitrided steel, performed with the open photoacoustic cell (OPC) technique (Prandel et al., 2013). The authors showed that the nitriding process resulted in an increase in the thermal diffusivity values, which may indicate that the sample will dissipate heat more quickly, therefore preventing it to propagate into the substrate.

This study presents mechanical and thermal characterization of Hastelloy X surfaces modified by plasma nitriding, aiming to promote better conditions for the deposition of other adjuvant coatings, such as TBC´s. The obtained layers comprised a range of compositions and microstructures, achieved by controlling the treatment parameters.

2. MATERIAL AND METHODS

2.1 Samples preparation

Hastelloy X discs with 3.5 cm diameter and 1 cm thickness were cut by wire electric discharge machining to the final thickness of 2 mm. After that, the raw samples (named as HXSB) were heat treated in a tubular oven at 1175 °C for 60 minutes and then quenched in cold water, according to the proper solubilization procedures described in Manoj et al. (2019) and Dithelmitz (2010). These samples were denominated as HXSLB.

The polishing was carried out equally on the sample´s both sides (front and back) in order to investigate the thermal effects on the bulk material due to nitriding. The pieces were grinded with SiC papers (P80 to P3000 mesh) and polished in alumina suspensions with particle sizes 1 μm and 0.03 μm. The final finish was mirrored and scratch-free surfaces, as expected (Mcdaniels, 2011).

2.2 DC Plasma nitriding

The system configuration, available at UEPG, is shown in Figure 1. In this system, the cathode temperature is controlled by the process variables and results from the balance of the plasma energy.

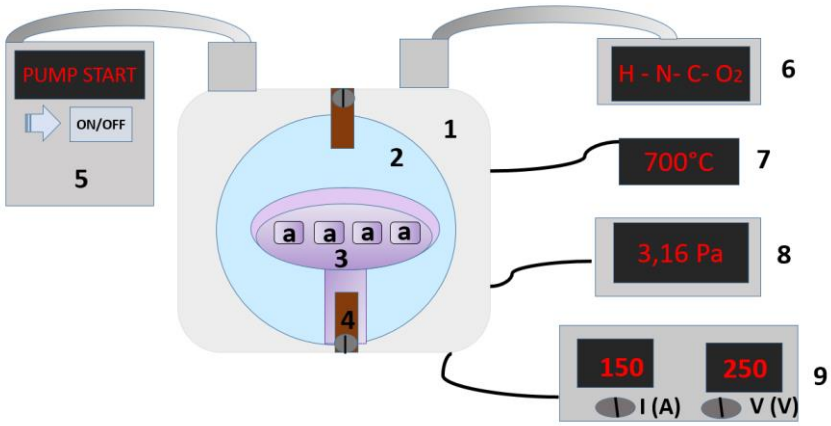

Figure 1. Scheme of the experimental apparatus of the GD plasma nitriding reactor: AISI316 steel vacuum chamber (1), optical window (2), sample/cathode holder (3), safety lock (4), vacuum pump (5), mixer/ gas controller (6), thermocouple (7), pressure controller (8), voltage and current source (9).

The nitriding was carried out on 12 solubilized samples at four different temperature conditions: 400°C, 500°C, 600°C and 700°C. Before nitriding, the surfaces and the chamber were purged by Ar + H_2 plasma sputtering for 30 minutes at 300 ºC. Then, the chamber was re-evacuated and the nitriding gas mixture, consisting of 50% N_2 + 50% H_2 by volume, was inserted. The treatment time was 3 h. Table 1 presents the nitriding parameters for each of the studied conditions. The control of each parameter was performed every 20 min.

Table 1. Average nitriding parameters, where GD represents the nitriding methodology on the face exposed to the treatment and GDT means the back face of the sample, not exposed to nitriding but only to heating. The values 400, 500, 600 and 700 ascribe to treatment temperatures. HXSLB refers to the only solubilized sample, while HXSB is the one received for analysis, with none treatment.

Sample name	tratament time (h)	Temperature (°C)	Pressure (Pa)	Current (mA)	Voltage (V)
GD400 GDT400	3h	400± 3	324 ± 0.6	268± 2	428 ± 1
GD500 GDT500	3h	500 ± 1	285 ± 0.8	333± 1	483 ± 1
GD600 GDT600	3h	600 ± 2	282 ± 0.9	422 ± 2	555 ± 1
GD700 GDT700	3h	701 ± 1	185 ± 0.7	527 ± 3	725 ± 1
HXSLB	-	-	-	-	-
HXSB	-	-	-	-	-

2.2 Structure and Microstructure

The morphology of the surfaces before and after nitriding, as well as the cross-section analysis of the modified layer, were analyzed using a field emission scanning electron microscope (Tescan Mira3) equipped with microanalysis by Energy Dispersive X-ray Spectroscopy - EDS (Oxford XMaxN SDD).

X-ray diffraction (XRD) was performed with a Rigaku Ultima IV diffractometer. The diffractograms were obtained with CuKα radiation (λ = 0.15406 nm) using the grazing incidence geometry, collected between 30 and 60° in continuous mode at a speed of 0.3°/min, with incidence angles fixed at 10°. This characterization was performed on both sides of the samples, that is, on the nitrided surface and on the opposite side facing the cathode, subject only to the thermal changes of the treatment.

The following PDF cards were employed for identification of the diffraction peaks: CrN 33-397, Cr_2N 35-803, γ 33-395, Ni_4N 36-1300, Ni_3Mo_3N 49-1336, Mo_2N 24-768.

2.3 Thermal diffusivity measurements with the two-beam phase-lag method

In the phase-lag method (T2F), developed in 1985 by Pessoa et al., the thermal diffusivity is obtained from a single chopping frequency measurement. Measuring relative phase lag (ΔΨ= ΦF – ΦR) at a single modulation frequency, between the rear-surface illumination ® and the front-surface illumination (F), it is possible to determine the thermal diffusivity of the material (Pessoa et al., 1986; Drabeski et al, 2020).

The experimental arrangement of two-beam experiment is the same as the one described in Drabeski et al. (2019) (Figure 2). The light from a solid state laser (650 nm, 300 mW red) is modulated by the lock-in amplifier (SR830, Stanford Research System) using the TTL logic signal, and modulated beam is directed on both sides of the photoacoustic (PA) cell. The planed-shaped sample is fixed with silicon gel to a conventional aluminum PA cell that has a 6-mm-diam hole through which the rear-side laser beam is incident. The BK condenser microphone (4943-L-001, Brüel & Kjaer) is mounted on one of the PA cell walls and connected to the amplifier.

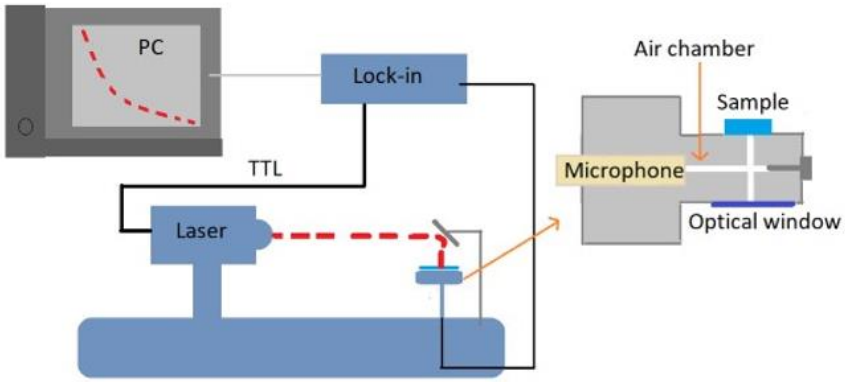

Figure 2. Experimental setup for the two-beam photoacoustic measurements of the thermal diffusivity (Drabeski et al., 2019).

The typical two beam PA phase lag are given by:

$$tan(\Delta\psi) = tanh(Z)tan(Z) \qquad (1)$$

with $Z = l_s a_s$, where: l_s=sample thickness; a_s=thermal diffusion length. One can evaluate the parameter Z from tan(Δψ) at a single frequency. The Hastelloy X samples were painted in black to ensure the opacity of the material. After measuring front signal phase (ΦF) and rear signal phase (ΦR), and knowing the thickness of the sample, the thermal diffusion coefficient (a_s) was determined. With a single measurement of the modulation frequency, it is possible to measure the thermal diffusivity of the material by:

$$\alpha = \pi f \left(\frac{l_s}{z}\right)^2. \qquad (2)$$

2.4 Mechanical properties

Hardness and elastic modulus were measured by nanoindentation (UNAT, ASMEC). The tests were carried out with a pyramidal diamond tip with the Berkovich geometry. The tip area function was determined by testing on silica and sapphire standards.

The equipment allows the use of loads from 0.02 mN to 2000 mN. In the layers produced in this work, after tests under different conditions, it was decided to use maximum loads of 400 mN, applied according to the QCSM (Quasi-Continuous Stiffness Measurement) method.

3. RESULTS AND DISCUSSION

3.1 Microestructural characterization

Analyses of the cross-sectioned nitrided samples, allowed to infer the modified layer thicknesses, in which nitrogen entered the interstitial positions of the superalloy, as well as the nitrogen content present in the material. Figure 4 presents nitrogen profiles, obtained by point EDS, for the four different treatment configurations.

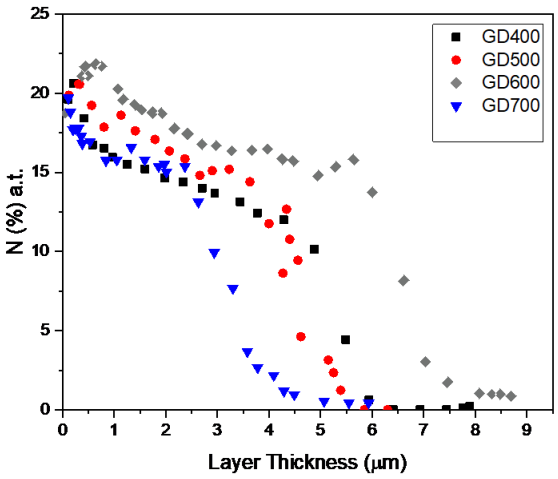

Figure 3. Nitrogen depth profiles of the nitrided layers, obtained by point EDS.

The nitrogen profiles in Figure 3 indicate a similar tendency, in all samples, to present approximately 20% N in the top surface region. The profile decayed as the layer depth increased. Plateaus were identified in which the N concentrations were approximately constant. The formation of the plateau is explained by the diffusion mechanism and nitrogen entrapment in solid solution in the austenitic structure. N occupies interstitial positions from the surface, just below the surface, the nitrogen diffusion process occurs in the crystal structure and new implanted N atoms searched for available interstices located below the surface layer, resulting in N trapping by the CFC matrix (Manova et al., 2017). From the depth 3 μm, the percentage of N drops up to approximately 5 μm, where the profiles tend to cease. The modified layers thicknesses can be inferred by assuming the middle of the dropping region as the interface with substrates. Thicknesses increased as the treatment temperature raised from 400 °C to 600 °C, which is expected for a diffusion-driven phenomenon. However, the layer on the GD700 sample diverged from this trend, since it showed an abrupt drop in the N content in a much shallower depth. Possibly, the decrease in thickness of the nitrided layer at 700°C can be related to two effects: *(i)* the sputtering process, which causes the surface to recess and is high-voltage dependent; and (ii) the achievement of thermodynamical conditions for a plenty of nitrides precipitation, specially chromium nitride, which retains and provides nitrogen to diffuse into the matrix.

Figure 4 presents the X-ray diffractograms. The solubilized Hastelloy X (HXSBL) disclosed only peaks ascribed to austenite, as expected. For each of the nitrided surface, Figure 4 shows diffractograms for their respective counter faces, not exposed to the plasma but only to the heating process. None significant differences from the HXSBL condition were observed. The main change was the peaks widths, larger than the solubilized condition. This may indicate superposition with peaks from precipitates and/or σ phase, though this cannot be clearly distinguished in the diffractograms. Concerning the nitrided surfaces shown in Figure 4, the diffractograms showed additional peaks, broader and adjacent (at lower 2θ) to those referring to the respective Hastelloy X substrates. They are due to the entry and accommodation of nitrogen in octahedral interstices of the FCC structure, causing residual compressive stresses. This phase is called the γ_n or the S-phase. In 2θ ~37.5° of the diffractogram, a superposition of S-phase peaks with precipitate peaks such as chromium nitrides (Cr_2N) may have occurred. Such compound formation is generally observed in nitriding with temperatures higher than 400°C in other nickel superalloys with significant amounts of Cr (Eliasen et al., 2010). Also noticeable is the significant broadening of the austenite peaks after nitriding, with a slight change of the peak maximum. It could indicate nitrogen in solid solution producing a first-order expansion phase, with lattice parameters closer to that from austenite and lower than those of the (second-order) S-phase. However, the XRD probe depth calculated by the X'Pert HighScore Plus tool was estimated to be 0.4 μm, which is the S-phase domain, as seen in Fig. 4. Again, a superposition with nitride peaks must explain it, now with contributions from the expanded phase of the subsequent crystal direction – i.e., the $\gamma_N(200)$ may contribute with the peak at the position expected for $\gamma(111)$ due to the high strains imposed to the lattice.

The peak overlap is also presented at ~44.3° where there are also contributions from chromium nitride and M_6C carbide (Sathishkumar et al, 2019). The treatment temperature directly influenced the diffusion of N in the material structure.

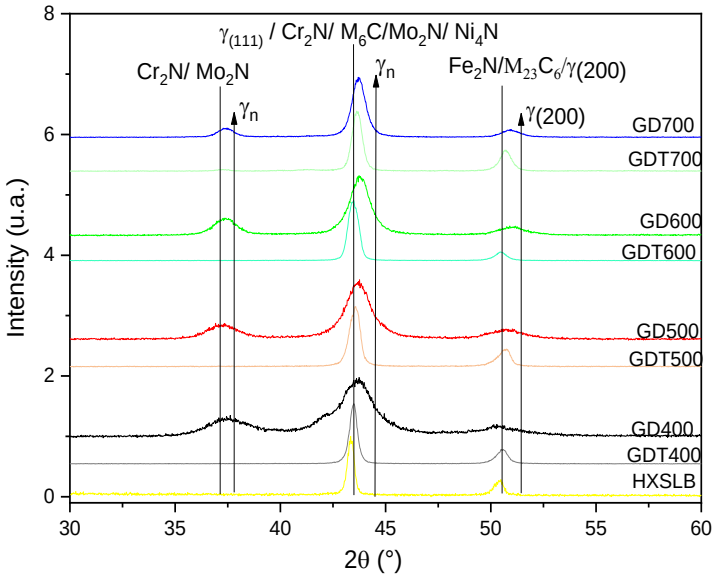

Figure 4- X-ray diffractograms for the Hastelloy X samples under the conditions: GD400, GD500, GD600, GD700 and their respective countersides (not nitrided), named GDT, γn represents the S phase. The diffractogram was performed with a fixed angle of 10°, except for HXSLB, for which the grazing angle was 5°.

3.2 Thermal diffusivity

The two-beam phase-lag measurements were performed seven times for each side of the sample in ten runs of 13 - 103 Hz modulation-frequency range. The photoacoustic signal amplitude was normalized by the microphone response function (Marquezini et al., 1991).

Figure 5 presents a typical the logarithm of the rear signal intensity as a modulation frequency function of 13-103 Hz for the Hastelloy X sample nitrided at 600°C. The $f^{-1.5}$ behavior shows that the region in which the thermal diffusion contribution (Rosencwaig and Gersho, 1976) predominates was between 13-38 Hz, and the phase-lag method is justified for determining the thermal difusivity. For high modulation frequencies, the thermoelastic mechanism (Vargas and Miranda, 1988) was predominant ($f^{-1.0}$).

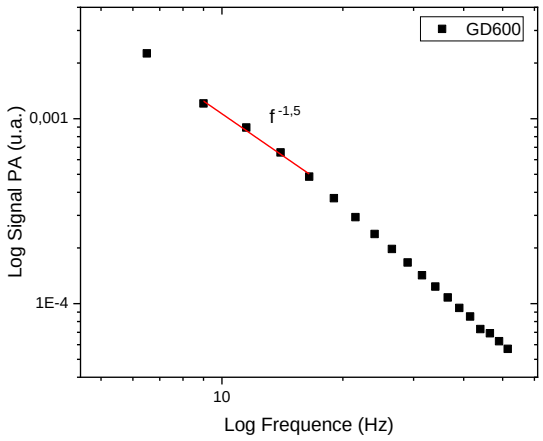

Figure 5. Typical log-log plot of PA rear-signal amplitude versus modulation frequency, for the sample GD600.

Table 2 presents the average effective thermal diffusivity of the samples. The experimental error on the b value was calculated by using the standard formula for error propagation.

Table 2. Experimental response of effective thermal diffusivity for nitrided and solubilized samples.

Sample	Average thermal diffusivity α (x10^{-6} m²/s)	Thickness (μm)
HXSLB	1.86 ± 0.02	1449
GD400	3.16 ± 0.02	1692
GD500	2.74 ± 0.03	1620
GD600	3.37 ± 0.05	1659
GD700	4.31 ± 0.04	1792

The thermal diffusivity of the nickel superalloy (HXSLB) was 1.86 x10^{-6} m²/s. After the nitriding process, the effective thermal diffusivity values increased as the treatment temperature increased, reaching values of 4.31x10^{-6} m²/s at 700°C the maximum nitriding temperature. Teixeira et al. (2011) estimated the thermal diffusivity for the nickel (Ni) as 14.9 x10^{-6} m²/s by NanoFlash method. On the other hand, similar to the thermal effective diffusivity value found here for the GD700 sample, Sundqvist (1992) using Angström's method at 26.85°C found a value of 4,7x10^{-6} m²/s for the commercially available Chromel contains 89%-90% Ni, 9%-9.5% Cr by weight, plus often minor amounts (well below 1% each) of Si, Fe, Mn, C, Co, and/or Nb.

It is noteworthy that studies related to the thermal diffusivity of nitrided layers of the Hastelloy X superalloy are not found in the literature, as well as the application of nitriding in aerospace components. The values found for the non-nitrided superalloy come from all the elements that make up the material, and other factors such as the material´s porosity and density, layer thickness and the structure constitution (Meloa et al., 2006).

The nitrided samples showed an increasing thermal diffusivity value with the treatment temperature. Prandel et al. (2013), who studied the thermal diffusivity of nitrided steels, reported a similar behavior.

The increase in thermal diffusivity indicates a faster propagation/dissipation of heat in the material (de Souza et al. (b), 2017). Yakout et al. (2020) studied the influence of thermal diffusivity in aerospace materials; their studies showed that high thermal diffusivity in the material reduces thermal stresses, ensuring a lower temperature differential in the part and, consequently, less thermal stress.

3.3 Mechanical Properties

Hardness (Figures 6) and elastic modulus (Figure 7) were evaluated for both the nitrided face and the opposite face of the samples, in order to infer the bulk effects on the surface properties of the treated material.

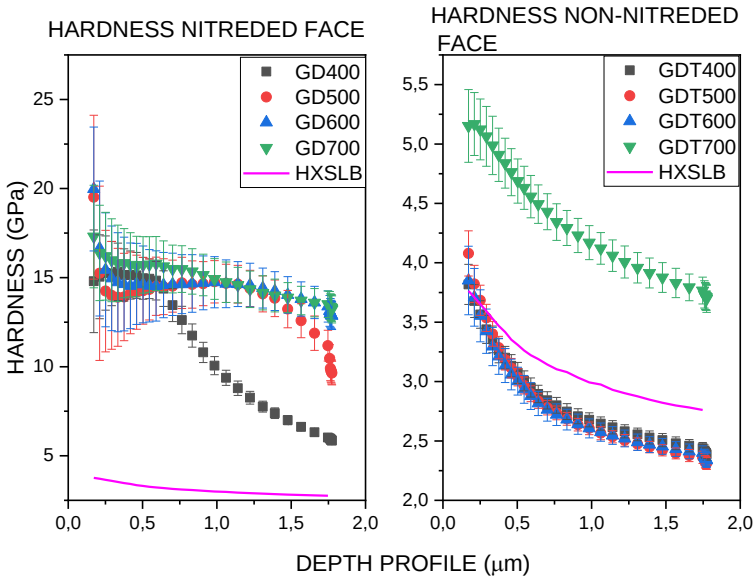

Figure 6. Hardness profiles for (a) the nitrided face (GD) and (b) the opposite face (GDT), subjected only to thermal effects from the treatment.

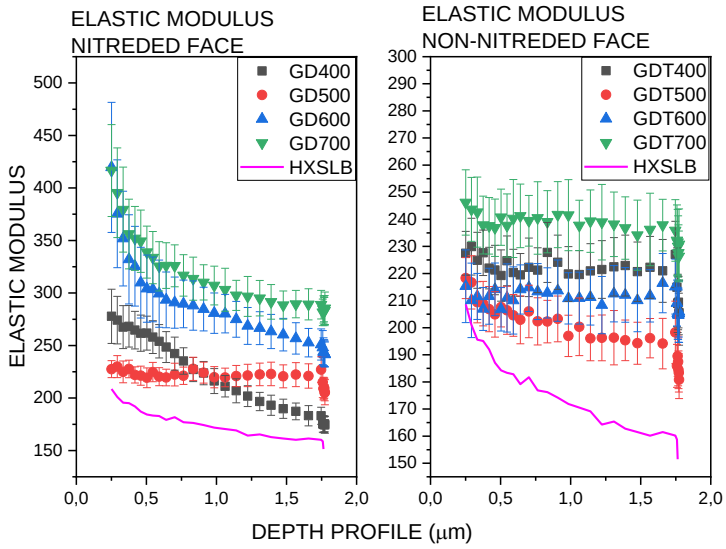

Figure 7. Elastic modulus profiles for (a) the nitrided face (GD) and (b) the opposite face (GDT), subjected only to thermal effects from the treatment.

All the samples had their hardness values increased after the nitriding at the face exposed to the plasma. The hardness profiles presented a higher level in the conditions GD600 and GD700 if compared with the samples GD400 and GD500, possibly a result of nitride precipitates formed in the modified layer, although this was not clearly identified by XRD. When measuring mechanical properties in thin modified layers, it is imperative to consider the substrate contributions, since the elasto-plastic field can reach regions much deeper than the indenter penetration depth (Fischer_Cripps, 2004). As seen in Fig. 6 (b), the thermal treatment provided by nitriding to the Hastelloy X bulk did not produce any effect in hardness for temperatures 400 °C to 600 °C. However, it was significant for the GDT700 sample, (Fig. 6 b). Such effect can be explained by the possible formation of the σ phase, presented in the phase diagram for the percentage of ~8% p. by Mo on Hastelloy X (Spitzer, Schloetter, Zerga, 2017). The expected effect in the nitrided layer would be higher than the one shown in Fig. 6 (a), since the GD700 nitrided surface presented composition similar to the GD600 (Fig. 4), but a harder substrate. Perhaps, the thin layer formed on the GD700 (Fig. 3) may explain this result.

Based on the range of plateaus, where hardness was approximately constant, it increased with increasing treatment temperature, in agreement with increasing thickness of modified layers (Dong, 2010; Kurelo, 2019). Usually, the plateaus correspond to 10% the layer thicknesses due to the constrained propagation of the plastic strain field (Fischer_Cripps, 2004). One can observe, by comparing Figs. 3 and 6(a) that this held only for the GD400 case. In the present situation, a multilayer zone can be the reason for such lack of correspondence. Even if nitride layers were not clearly identified over S-phase rich regions, they were present in those surfaces prepared at high temperatures, namely from 500 °C on. Hence, the propagation of the plastic field was complex instead of being due to a single and uniform layer.

Contrarily to hardness, the elastic modulus profiles are influenced by the material's substrate at any depth, so plateaus were not observable in Fig. 7(a). The elastic modulus is a measure of the elastic deformation of the material directly associated with the bond between adjacent atoms/molecules (Fischer-Cripps, 2004). Thus, the effects seen in the substrates (Fig. 7b) reflects different phases in the bulk material. It must be investigated further to a proper correlation with XRD results.

4. CONCLUSIONS

Surfaces of the Hastelloy X nickel superalloy were DC plasma nitrided for the first time in this study. The treatment produced surface layers with the expanded austenite phase (the S-phase) in all the investigated temperatures, being it predominant in the treatment carried out at 400 °C. Higher temperatures (500-700 °C) also led to the formation of metal nitrides such as the Cr_2N. The nitrogen diffusion in the matrix, and the subsequent layer thicknesses, obeyed a complex and dynamic correlation with temperature due to the competitive nitrogen retention in interstices and precipitates. Because of this, the nitriding at 600 °C resulted in the thickest layer (8 μm) and the highest nitrogen amount at the top surface (20 at%).

The thermal effects from the nitriding process on the bulk material were also investigated at the opposite samples faces, not exposed to the plasma. Hardness varied only for the 700 °C condition, from 3.8 to 4.3 GPa, possibly due to

the formation of the S-phase. On the other hand, the nitriding produced cases with significant resistance to plastic deformation, with hardness values ranging from 10.5 GPa at the 400 °C treatment to ~14 GPa at the remaining ones.

The measured indentation elastic modulus of the nitrided surfaces increased as well. The thermal diffusivity of the nickel superalloy was 1.86 $x10^{-6}$ m^2/s. After the nitriding process, the effective thermal diffusivity values increased as the treatment temperature increased, reaching values of $4.31x10^{-6}$ m^2/s at the maximum nitriding temperature (700°C), a value similar to that of commercially available Chromel. This result is of intrinsic importance for heating dissipation at working conditions.

5. ACKNOWLEDGEMENTS

The authors are grateful to CNPq process 141959/2020-7, CAPES, C-LABMU/PROPESP and C²MMa - UTFPR.

6. REFERENCES

Alves JR, C. 2001. *Nitretação a Plasma: Fundamentos e Aplicações*. Natal: EDUFRN, 1and edition.

Carvalho, A.P.N., *et al.*, 2013. "In vitro thermal diffusivity measurements as aging process study in human tooth hard tissues". *Journal of Applied Physics*, Vol. 114, pp. 194705.

Ceccarelli, M. 2008. (Ed.). *Robot Manipulators*. BoD–Books on Demand. Intech Open, Croatia, 1and edition.

DE Souza (b), J. S. et al. 2017. *Thermal Characterization Of Hardmetal By Open Photoacoustic Cell Technique*. In: COBEM-2017-0352. Curitiba.

Diltemiz; S. F., Zhang, S., 2013. Superalloys for superjobs, in: S. Zhang, D. Zhao (Eds.), *Aerosp. Mater. Handb*., Taylor & Francis, Boca Raton, pp. 2–75.

Dong, H. 2010. S-phase surface engineering of Fe-Cr, Co-Cr and Ni-Cr alloys. International *Materials Reviews*, Vol. 55, n. 2, pp. 65–98.

Drabeski, R. G. 2019. *Desenvolvimento de filmes finos de dióxido de estanho depositados via spin-coating e caracterização das propriedades mecânicas e termo-ópticas*. Masther's Thesis. Universidade Tecnológica Federal do Paraná. Ponta Grossa, Brasil.

Drabeski, R. G., Gunha, J.V., Novatski, A., De Souza, G. B., Tebcherani, S. M., Kubaski, E. T., Dias, D. T. . 2020. Raman and photoacoustic spectroscopies of SnO_2 thin films deposited by spin coating technique. *Vibrational Spectroscopy*, Vol. 109, pp. 103094.

Eliasen, K. M.; Christiansen, T. L.; Somers, M., AJ. 2010. Low temperature gaseous nitriding of Ni based superalloys. *Surface Engineering*, v. 26, n. 4, p. 248-255. Eriksson, Robert. 2013 *Thermal barrier coatings: Durability assessment and life prediction*.. Ph.D. Thesis. Linköping University Electronic Press.

Fischer-Cripps, A. C. 2004. *Nanoindentation*. New York: Springer-Verlag.

Haynes International. 2019. *Principal Features HASTELLOY ® X alloy*, 06002.

He, J.; Lavernia, E. J. 2001. Development of nanocrystalline structure during cryomilling of Inconel 625. *Journal of Materials Research*, v. 16, n. 9, pp. 2724-2732.

KURELO, B. C. E. S. 2019. *Estudo do comportamento tribo-mecânico e da resistência a corrosão de superfícies nitretadas de aços inoxidáveis aplicados na indústria do petróleo e gás*. 2019. Ph.D.Thesis - Universidade Estadual de Ponta Grossa, Ponta Grossa, Brasil.

Kovací, H., Ghahramanzadeh, H. ASL, Çigdem, A., Akgün A., Ayhan C. 2016. Effect of plasma nitriding parameters on the wear resistance of alloy Inconel 718. *Metal Science and Heat Treatment*, v. 58, n. 7, pp. 470-474.

Kovářík, O., Haušild, P., Čapek, J., Medřický, J. 2016. Damping measurement during resonance fatigue test and its application for crack detection in TBC samples. In: *International Journal of Fatigue*. 2016. Vol. 82, pp. 300-309.

Leroy, C., Czerwiek, T., Gabet, C. 2001. Plasma assisted nitriding of Inconel 690. *Surface and Coatings Technology*, Vol. 142, pp. 241-247.

Limar, C. R. C. 2014. Revestimentos para barreira térmica: evolução e perspectivas. *Soldagem & Inspeção*, Vol. 19, n. 4, pp. 353-363.

Marquezini, M. V. et al. 1991. Open photoacoustic cell spectroscopy. *Measurement Science and Technology*, Vol. 2, n. 4, pp. 396.

Meola, C., Carlomagno, M., Squilacce, A. 2006. Non-destructive evaluation of aerospace materials with lock-in thermography. *Engineering failure analysis*, Vol. 13, n. 3, pp. 380-388.

Mcdaniels, R. L., Chen, L., Liaw AP. 2011. The strain-controlled fatigue behavior and modeling of Haynes® HASTELLOY® C-2000® superalloy. *Materials Science and Engineering: A*, Vol. 528, n. 12, pp. 3952-3960.

Manoj, I. V.; Joy, R.; Narendranath, S. 2020. Investigation on the effect of variation in cutting speeds and angle of cut during slant type taper cutting in WEDM of Hastelloy X. *Arabian Journal for Science and Engineering*, Vol. 45, n. 2, pp. 641-651.

Manova, D., Mandhl, L., Neumann H. 2017. Formation of metastable diffusion layers in Cr-containing iron, cobalt and nickel alloys after nitrogen insertion. *Surface and Coatings Technology*, Vol. 312, pp. 81-90.

Martins, M.; Casteletti, L. C. 2005. Heat treatment temperature influence on ASTM A890 GR 6A super duplex stainless steel microstructure. *Materials characterization*, Vol. 55, n. 3, pp. 225-233.

Mouritz, A. P. *Introduction to aerospace materials*, Woodhead Publishing, Oxford, 2012.

Parker, W. J. 1961. Laser flash method of determining thermal diffusivity, heat capacity and thermal conductivity. *J. Appl. Phys*., Vol. 32, pp. 1679-1684.

Prandel, L. V., Sommer, A., Asmann, A. 2013. Plasma nitriding process by direct current glow discharge at low temperature increasing the thermal diffusivity of AISI 304 stainless steel. *Journal of Applied Physics*, Vol. 113, n. 6, p. 063507.

Pessoa, O. Jr. 1985. *Aplicações de medidas de fase do efeito fotoacústico*, 1985. Ph.D. Thesis - Universidade Estadual de Campinas, Campinas, Brasil.

Pessoa JR, O. et al. 1986. Two-beam photoacoustic phase measurement of the thermal diffusivity of solids. *Journal of applied physics*, Vol. 59, n. 4, pp. 1316-1318.

Rosencwaig, A.; Gersho, A. 1976. Theory of the photoacoustic effect with solids. *Journal of Applied Physics*, Vol. 47, n. 1, pp. 64-69.

Sathishkumar, M.; Manikandan, M.; Arivazhagan, N. 2021. Prospects of pulsed current arc welding on aerospace grade Hastelloy X. *Proceedings of the Institution of Mechanical Engineers, Part E: Journal of Process Mechanical Engineering*, Vol. 235, n. 4, pp. 1059-1072.

SUNDQVIST, B. 1992. Thermal diffusivity and thermal conductivity of Chromel, Alumel, and Constantan in the range 100–450 K. *Journal of applied physics*, Vol. 72, n. 2, pp. 539-545.

Sfar, K.; Aktaa, J.; Munz, 2002. D. Numerical investigation of residual stress fields and crack behavior in TBC systems. *Materials Science and Engineering: A*, Vol. 333, n. 1-2, pp. 351-360.

Spitzer, J. A.; Schloetter, J. T.; Zerga, S. 2017. *Effect of Composition and Build Direction on Additively Manufactured Hastelloy X Alloys*. Masther's Thesis – Universidade Estadual Politécnica da Califórnia, San Luiz.

Takahashi, R. J., Assis, J. M. K., Piorino, F., Reis, D. A., 2019. Heat treatment for TGO growth on NiCrAlY for TBC application. *Materials Research Express*, Vol. 6, n. 12, pp. 126442.

TEIXEIRA, R. L. P. et al. 2011. Temperature influence on the thermal and structural properties of electrodeposited nanostructured black nickel cermet on high conductive C81100 copper. *International Journal of Low-Carbon Technologies*, Vol. 6, n. 1, pp. 86-92.

Ueda, M, Pillaca E. J., Mariano, S. M. 2014. *PIII and PIII&D treatments for the protection of the inside walls of metallic tubes of different diameters for petroleum, chemical, food and aerospace applications*. p; 13. Brazilian SBPMat meeting; Joao Pessoa, PB (Brazil).

Ueda, M. 2016. Novo método de implantação iônica por imersão em plasma e também deposição de componentes industriais utilizando fixação tubular e plasma gerado dentro do tubo por pulsos de alta tensão. *Review of Scientific Instruments* , Vol. 87, n. 1, pp. 013902.

Vargas, H., Miranda, L. C. M. 1988. Photoacoustic and related photothermal techniques. *Physics Reports*. Vol. *161, n.* 2, pp. 43-101.

Wang, G., Zheng J., Xu, B., Zhu, Y., 2021 . Tailored Electronic Band Gap and Valance Band Edge of Nickel Oxide via p-Type Incorporation. *The Journal of Physical Chemistry C*, Vol. 125, n. 13, pp. 7495-7501.

Yakout, M., Elbestawi Ma., Veldhuis, S. 2019. Influence of thermal properties on residual stresses in SLM of aerospace alloys. *Rapid Prototyping Journal*. Vol. 26, n. 1, pp.213-222.

Zhang, Q.; Meng, L.. Yin , X., Wang, L. 2021. Effects of Heat Treatment on High Temperature Mechanical Property and Corrosion Resistance of Hastelloy X Manufactured by Selective Laser Melting. *Nano*, Vol. 16, N.13, pp. 2150153.